DISCRETE AND CONTINUOUS
DYNAMICAL SYSTEMS–SERIES B
Volume **4**, Number **1**, February **2004**

Website: http://AIMsciences.org

pp. **99–114**

A MATHEMATICAL MODEL OF BCR-ABL AUTOPHOSPHORYLATION, SIGNALING THROUGH THE CRKL PATHWAY, AND GLEEVEC DYNAMICS IN CHRONIC MYELOID LEUKEMIA

Pep Charusanti[1], Xiao Hu[2], Luonan Chen[2], Daniel Neuhauser[1], and Joseph J. DiStefano III[2]

[1]Department of Chemistry and Biochemistry
University of California, Los Angeles, Los Angeles, California 90095-1569

[2]Biocybernetics Laboratory
Departments of Computer Science and Medicine
University of California, Los Angeles, Los Angeles, California 90095-1596

Abstract. A mathematical model is presented that describes several signaling events that occur in cells from patients with chronic myeloid leukemia, i.e. autophosphorylation of the Bcr-Abl oncoprotein and subsequent signaling through the Crkl pathway. Dynamical effects of the drug STI-571 (Gleevec) on these events are examined, and a minimal concentration for drug effectiveness is predicted by simulation. Most importantly, the model suggests that, for cells in blast crisis, cellular drug clearance mechanisms such as drug efflux pumps dramatically reduce the effectiveness of Gleevec. This is a new prediction regarding the efficacy of Gleevec. In addition, it is speculated that these resistance mechanisms might be present from the onset of disease.

1. **Introduction.** Chronic myeloid leukemia (CML) is a proliferative disorder of the blood system characterized by the increased production and accumulation of cells from the myeloid lineage. Though this lineage encompasses many cell types such as red blood cells, platelets, monocytes, and neutrophils, the neutrophil cell type is most affected (Figure 1). Indeed, patients with CML often have blood neutrophil concentrations a hundred to a thousand times above normal. All blood cells originate from a small pool of hematopoietic stem cells in the bone marrow. Thus, the origin of the elevated neutrophil count, and the origin of the disease, is a small pool of malignant stem cells that exhibit deregulated proliferation [19,25,27,43].

CML progresses through three stages. The initial chronic phase is characterized by the overproduction of granulocytes. Non-leukemic granulocytes continue to be produced, and both leukemic and non-leukemic cells mature fully. This phase typically lasts 3-5 years from diagnosis. An intermediate accelerated phase of 6-18 months follows. Lastly, blast crisis occurs, a stage in which the production of non-leukemic granulocytes disappears as the production of leukemic granulocytes dominates. In addition, a higher percentage of the leukemic granulocytes produced are immature, non-functional cells. Prognosis during blast crisis is usually poor, with a median duration to mortality of only 3-6 months [31,39].

2000 *Mathematics Subject Classification.* 92C45, 92B05.

Key words and phrases. chronic myeloid leukemia, bcr-abl, Gleevec, clearance, autophosphorylation.

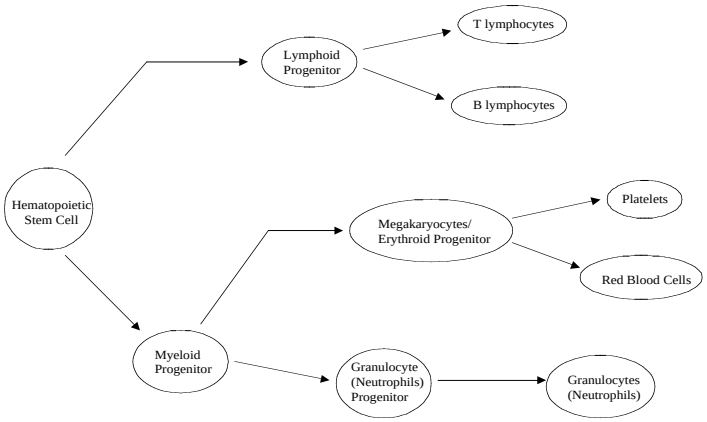

FIGURE 1. Hematopoiesis. Blood cells of all types originate from a small pool of hematopoietic stem cells in the bone marrow. The two major lineages are the myeloid lineage and the lymphoid lineage. Each lineage is further divided into more specialized cell types.

At the molecular level, the hallmark of CML can be traced to a single mutation: the presence of the Philadelphia (Ph) chromosome in myeloid cells at all stages of differentiation. This chromosome is created by the translocation of a region of chromosome 9 with a region of chromosome 22 [38]. Chromosomes contain genes, and genes encode proteins. The major protein that corresponds to the Ph chromosome is Bcr-Abl, and is present in >90% of cases of CML [3,10,15,51].

Functionally, Bcr-Abl acts as a kinase enzyme, catalyzing the addition of phosphate groups to various substrate molecules, but in a deregulated manner, whereas cell signaling is normally a carefully regulated process. Enzymes become activated and inactivated in response to both extracellular and intracellular conditions. In response, different signaling pathways become activated or inactivated. Bcr-Abl abrogates this on/off control mechanism by continually activating multiple signaling pathways, pathways linked, for example, to the control of cellular proliferation and cell death. Signaling pathways constitutively activated by Bcr-Abl include: the Ras pathway [31,36], the Jun-kinase pathways [37], the PI3K pathway [45], and the Jak-STAT pathway [8,14,26].

That Bcr-Abl alone is sufficient to cause CML has been experimentally established [13], and represents a unique feature of CML. The cause of most cancers usually cannot be traced back to the presence of a single genetic abnormality, as in CML. Instead, for most cancers, a multitude of defects arise at both the genetic and molecular level, obscuring the underlying mechanism for the transformation of a cell from the normal state to a cancerous state. Because of the unique role that Bcr-Abl plays in CML, research efforts aimed at treating CML have logically targeted Bcr-Abl and its enzymatic activity. Therapies based on this strategy have already proven themselves as viable treatments for CML. In particular, recent clinical trials

of the compound STI-571, branded Gleevec by the drug company Novartis, have demonstrated remarkable efficacy at inhibiting Bcr-Abl and inducing remission in patients with CML [11,18,28].

We present a mathematical model here that describes Bcr-Abl autophosphorylation and signaling through the Crkl pathway. The main result derived from this model is that drug clearance by the cell during blast crisis is very rapid, leading to reduced drug effectiveness. In addition, it is speculated that this mechanism(s) might be present even before therapy begins. Lastly, results of a phase plane analysis predict a minimal value for the cellular concentration of Gleevec required for efficacy.

2. **Mathematical Model.** Our model contains two main components. This first is Bcr-Abl autophosphorylation. Unphosphorylated Bcr-Abl binds reversibly to ATP to form a Bcr-Abl·ATP complex, which then encounters a second Bcr-Abl·ATP complex to cross-phosphorylate Bcr-Abl. This phosphorylated form of Bcr-Abl is denoted Bcr-Abl*. Simulation results from this portion of the model can be compared to mouse experimental Bcr-Abl autophosphorylation data [29].

The second component of the model is Bcr-Abl signaling through the Crkl pathway. Bcr-Abl* binds a molecule of ATP. At this point, the Bcr-Abl*·ATP complex binds Crkl, transferring to Crkl a phosphoryl group from ATP. Finally, the Bcr-Abl*·ADP·Crkl breaks apart to give Bcr-Abl*, ADP, and phosphorylated Crkl, denoted Crkl*.

Crkl signaling is included here because the phosphorylation level of Crkl provides an indirect measure of Bcr-Abl activity in human cells. Bcr-Abl autophosphorylation levels cannot be measured directly from human cells obtained in the clinic [23], so an indirect measure must be used. This indirect measure is taken to be the percentage of phosphorylated Crkl molecules; Crkl is a known substrate of Bcr-Abl [34,35,48]. In normal human cells, the percentage of phosphorylated Crkl molecules is approximately 25%-30%, but in leukemic cells it is over 70% [23]. To make our model more relevant for human data then, we have included Bcr-Abl signaling through the Crkl pathway. It must be emphasized, however, that examining Bcr-Abl signaling through the Crkl pathway is not the main goal of our model since no experimental time-concentration data exists with which this portion of the model can be validated. The Crkl pathway has therefore been included in anticipation that such time course data from human cells obtained in the clinic will become available in the future.

A diagram of the complete network of Bcr-Abl autophosphorylation and Crkl signaling is presented in Figure 2. Figure 3 illustrates how Gleevec acts as a competitive inhibitor of ATP for both Bcr-Abl and Bcr-Abl* [40].

The diagram in Figure 2 is translated into the following set of ordinary differential equations using standard principles of biochemical kinetics.

$$\begin{aligned}\frac{d[\text{Bcr-Abl}]}{dt} &= S_0 - k_1[\text{Bcr-Abl}][\text{ATP}] + k_{-1}[\text{Bcr-Abl·ATP}] \\ &\quad + k_{\text{deph1}}[\text{Bcr-Abl*}] - k_{\text{deg1}}[\text{Bcr-Abl}] \\ &\quad - k_{\text{I1}}[\text{Bcr-Abl}][\text{G}] + k_{-\text{I1}}[\text{Bcr-Abl·G}] \end{aligned} \tag{1}$$

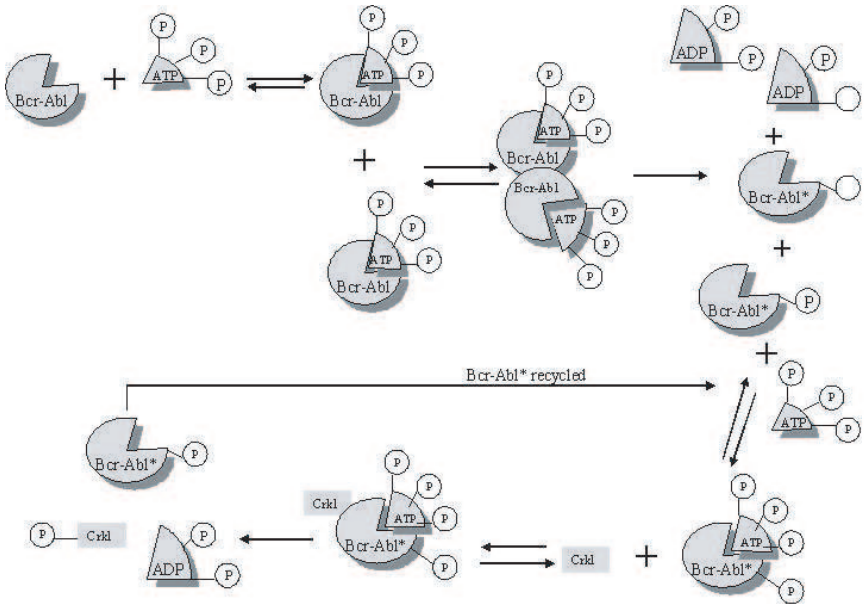

FIGURE 2. Bcr-Abl autophosphorylation and signaling through the Crkl pathway. The first step in all Bcr-Abl mediated cell signaling events is the binding of ATP to Bcr-Abl. Two such molecules then cross-phosphorylate each other to produce an activated, phosphorylated form of Bcr-Abl, denoted Bcr-Abl* and two molecules of ADP. Bcr-Abl* then binds a second ATP molecule, after which it can bind a number of substrates. One such substrate is Crkl. The Bcr-Abl*·ATP complex phosphorylates Crkl, which then propagates the signal through the rest of cell.

$$\begin{aligned}\frac{d[\text{Bcr-Abl}\cdot\text{ATP}]}{dt} &= k_1[\text{Bcr-Abl}][\text{ATP}] - k_{-1}[\text{Bcr-Abl}\cdot\text{ATP}] \\ &\quad -k_{1\text{A}}[\text{Bcr-Abl}\cdot\text{ATP}]^2 \\ &\quad +k_{-1\text{A}}[\text{Bcr-Abl}\cdot\text{ATP}\bullet\text{Bcr-Abl}\cdot\text{ATP}] \end{aligned} \tag{2}$$

$$\begin{aligned}\frac{d[\text{Bcr-Abl}\cdot\text{ATP}\bullet\text{Bcr-Abl}\cdot\text{ATP}]}{dt} &= k_{1\text{A}}[\text{Bcr-Abl}\cdot\text{ATP}]^2 \\ &\quad -k_{-1\text{A}}[\text{Bcr-Abl}\cdot\text{ATP}\bullet\text{Bcr-Abl}\cdot\text{ATP}] \\ &\quad -k_{\text{auto}}[\text{Bcr-Abl}\cdot\text{ATP}\bullet\text{Bcr-Abl}\cdot\text{ATP}] \end{aligned} \tag{3}$$

$$\begin{aligned}\frac{d[\text{Bcr-Abl*}]}{dt} &= k_{\text{auto}}[\text{Bcr-Abl}\cdot\text{ATP}\bullet\text{Bcr-Abl}\cdot\text{ATP}] - k_{1\text{B}}[\text{Bcr-Abl*}][\text{ATP}] \\ &\quad +k_{-1\text{B}}[\text{Bcr-Abl*}\cdot\text{ATP}] - k_{\text{I2}}[\text{Bcr-Abl*}][\text{G}] \\ &\quad +k_{-\text{I2}}[\text{Bcr-Abl*}\cdot\text{G}] + k_{\text{ph}}[\text{Bcr-Abl*}\cdot\text{ATP}\cdot\text{Crkl}] \end{aligned} \tag{4}$$

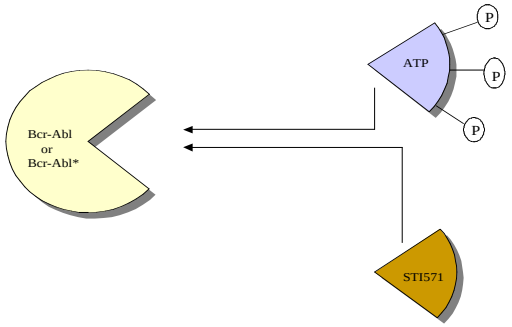

FIGURE 3. Current understanding of the mechanism of action of Gleevec (STI571). Gleevec is a competitive inhibitor of ATP for the ATP binding site in both Bcr-Abl and Bcr-Abl*, though the drug binds more strongly the unphosphorylated form, Bcr-Abl. Binding of ATP to Bcr-Abl and Bcr-Abl* is crucial to Bcr-Abl induced deregulated cell signaling.

$$\begin{aligned}\frac{d[\text{Bcr-Abl}\cdot\text{ATP}]}{dt} &= k_{1\text{B}}[\text{Bcr-Abl*}][\text{ATP}] \\ &\quad -k_{-1\text{B}}[\text{Bcr-Abl*}\cdot\text{ATP}] \\ &\quad -k_2[\text{Bcr-Abl*}\cdot\text{ATP}][\text{Crkl}] + k_{-2}[\text{Bcr-Abl*}\cdot\text{ATP}\cdot\text{Crkl}] \end{aligned} \tag{5}$$

$$\begin{aligned}\frac{d[\text{Bcr-Abl}\cdot\text{ATP}\cdot\text{Crkl}]}{dt} &= k_2[\text{Bcr-Abl*}\cdot\text{ATP}][\text{Crkl}] \\ &\quad -k_{-2}[\text{Bcr-Abl*}\cdot\text{ATP}\cdot\text{Crkl}] \\ &\quad -k_{\text{ph}}[\text{Bcr-Abl*}\cdot\text{ATP}\cdot\text{Crkl}] \end{aligned} \tag{6}$$

$$\begin{aligned}\frac{d[\text{Crkl}]}{dt} &= S_1 - k_{\text{deg}5}[\text{Crkl}] - k_2[\text{Bcr-Abl*}\cdot\text{ATP}][\text{Crkl}] \\ &\quad +k_{-2}[\text{Bcr-Abl*}\cdot\text{ATP}\cdot\text{Crkl}] + k_{\text{deph}2}[\text{Crkl*}] \end{aligned} \tag{7}$$

$$\frac{d[\text{Crkl*}]}{dt} = S_2 + k_{\text{ph}}[\text{Bcr-Abl*}\cdot\text{ATP}\cdot\text{Crkl}] - k_{\text{deph}2}[\text{Crkl*}] \tag{8}$$

$$\frac{d[\text{Bcr-Abl}\cdot\text{G}]}{dt} = k_{\text{I}1}[\text{Bcr-Abl}][\text{G}] - k_{-\text{I}1}[\text{Bcr-Abl}\cdot\text{G}] \tag{9}$$

$$\frac{d[\text{Bcr-Abl*}\cdot\text{G}]}{dt} = k_{\text{I}2}[\text{Bcr-Abl*}][\text{G}] - k_{-\text{I}2}[\text{Bcr-Abl*}\cdot\text{G}] \tag{10}$$

2.1. **Notation.** [...] represents cellular concentration in nM of a particular species. S_0 and S_1 are the synthesis rates of Bcr-Abl and Crkl from DNA transcription and subsequent mRNA translation, respectively. S_2 is the background phosphorylation rate of Crkl to produce Crkl*.

2.2. **Model Assumptions.** First, we assume that the concentration of ATP, denoted [ATP], is constant.

Second, we assume that the phosphorylation of Crkl by inactive Bcr-Abl is negligible in comparison to the phosphorylation of Crkl by activated Bcr-Abl*. Phosphorylation reactions require that the enzyme initially bind ATP. The rate with which ATP binds to the unphosphorylated, inactive form of Bcr-Abl is a thousand times lower than the rate with which it binds to the active, phosphorylated form [40].

Third, we assume that autophosphorylation of Bcr-Abl proceeds via a cross-phosphorylation mechanism whereby two molecules of Bcr-Abl·ATP bind to each other and a phosphoryl group from ATP is transferred from one complex to the other. Though autophosphorylation can also occur via an intramolecular mechanism, kinetic experiments involving the catalytic domain of murine Bcr-Abl more strongly support a cross-phosphorylation mechanism [6].

Fourth, we assume linear degradation for all species. Currently there are two known mechanisms of protein degradation. The first consists of enzyme-mediated attachment of a ubiquitin chain to proteins, which are then recognized and targeted for degradation by proteasomes [22]. The second is mediated by enzymes in cellular organelles called lysosomes [12]. Though both mechanisms could give rise to nonlinear degradation dynamics, we assume that the concentrations of any enzyme involved in protein degradation remains sufficiently constant such that the dynamics can be taken as first order. In a similar manner, we assume that all dephosphorylation reactions are also first order.

Fifth, we assume that the rate of binding and phosphorylation of two Bcr-Abl·ATP molecules during cross-phosphorylation is much faster than the rate of release of products from the Bcr-Abl*·ATP•Bcr-Abl*-ATP complex ($k_{\text{auto}} << k_{1A}$). Exact numerical values for k_{auto} and k_{1A} are not known for this particular reaction, so we base this assumption on published rate constants for similar binding, phosphorylation and product release reactions mediated by other kinase enzymes [9,44,52]. Similarly, we assume that the rate of binding and phosphorylation of Crkl by the Bcr-Abl*·ATP complex is much more rapid than the rate of release of products from the Bcr-Abl*·ATP·Crkl complex ($k_{\text{ph}} << k_2$). These two assumptions imply that the concentration of [Bcr-Abl·ATP•Bcr-Abl·ATP] and [Bcr-Abl*·ATP·Crkl] reach pseudo-steady state relative to the other reactions in the system. Setting the rate equations for these two species to zero and making appropriate substitutions leads to the following reduced set of equations.

$$\begin{aligned}\frac{d[\text{Bcr-Abl}]}{dt} &= S_0 - k_1[\text{Bcr-Abl}][\text{ATP}] + k_{-1}[\text{Bcr-Abl·ATP}] \\ &\quad + k_{\text{deph1}}[\text{Bcr-Abl*}] - k_{\text{deg1}}[\text{Bcr-Abl}] \\ &\quad - k_{\text{I1}}[\text{Bcr-Abl}]\left(\left(\frac{10^9}{59}\right)G^m_{cell}\right) + k_{\text{-I1}}[\text{Bcr-Abl·G}] \qquad (11)\end{aligned}$$

$$\frac{d[\text{Bcr-Abl}\cdot\text{ATP}]}{dt} = k_1[\text{Bcr-Abl}][\text{ATP}] - k_{-1}[\text{Bcr-Abl}\cdot\text{ATP}] - \frac{k_{1\text{A}}k_{\text{auto}}}{k_{-1\text{A}}+k_{\text{auto}}}[\text{Bcr-Abl}\cdot\text{ATP}]^2 \quad (12)$$

$$\frac{d[\text{Bcr-Abl}^*]}{dt} = \frac{k_{1\text{A}}k_{\text{auto}}}{k_{-1\text{A}}+k_{\text{auto}}}[\text{Bcr-Abl}\cdot\text{ATP}]^2 - k_{1\text{B}}[\text{Bcr-Abl}^*][\text{ATP}] + \frac{k_{\text{ph}}k_2}{k_{\text{ph}}+k_{-2}}[\text{Bcr-Abl}^*\cdot\text{ATP}][\text{Crkl}] - k_{\text{deph1}}[\text{Bcr-Abl}^*] + k_{\text{I2}}[\text{Bcr-Abl}^*]\left(\left(\frac{10^9}{59}\right)G^m_{cell}\right) + k_{-\text{I2}}[\text{Bcr-Abl}^*\cdot\text{G}] \quad (13)$$

$$\frac{d[\text{Bcr-Abl}\cdot\text{ATP}]}{dt} = k_{1\text{B}}[\text{Bcr-Abl}^*][\text{ATP}] - k_{-1\text{B}}[\text{Bcr-Abl}^*\cdot\text{ATP}] - \frac{k_{\text{ph}}k_2}{k_{\text{ph}}+k_{-2}}[\text{Bcr-Abl}^*\cdot\text{ATP}][\text{Crkl}] \quad (14)$$

$$\frac{d[\text{Crkl}]}{dt} = S_1 - \frac{k_{\text{ph}}k_2}{k_{\text{ph}}+k_{-2}}[\text{Bcr-Abl}^*\cdot\text{ATP}][\text{Crkl}] + k_{\text{deph2}}[\text{Crkl}^*] - k_{\text{deg2}}[Crkl] \quad (15)$$

$$\frac{d[\text{Crkl}^*]}{dt} = S_2 + \frac{k_{\text{ph}}k_2}{k_{\text{ph}}+k_{-2}}[\text{Bcr-Abl}^*\cdot\text{ATP}][\text{Crkl}] - k_{\text{deph2}}[\text{Crkl}^*] \quad (16)$$

$$\frac{d[\text{Bcr-Abl}\cdot\text{G}]}{dt} = k_{\text{I1}}[\text{Bcr-Abl}][\text{G}] - k_{-\text{I1}}[\text{Bcr-Abl}\cdot\text{G}] \quad (17)$$

$$\frac{d[\text{Bcr-Abl}^*\cdot\text{G}]}{dt} = k_{\text{I2}}[\text{Bcr-Abl}^*][\text{G}] - k_{-\text{I2}}[\text{Bcr-Abl}^*\cdot\text{G}] \quad (18)$$

$$\frac{dG^m_{IP}}{dt} = U - k_{21}G^m_{IP} \quad (19)$$

$$\frac{dG^m_{bl}}{dt} = k_{21}G^m_{IP} - k_{32}G^m_{bl} + k_{23}G^m_{cell} - k_{02}G^m_{bl} \quad (20)$$

$$\frac{dG^m_{cell}}{dt} = k_{32}G^m_{bl} - k_{23}G^m_{cell} - k_{\text{deg3}}G^m_{cell} - k_{\text{I1}}\left(\left(\frac{59}{10^9}\right)[\text{Bcr-Abl}]\right)G^m_{cell} + k_{-\text{I1}}\left(\left(\frac{59}{10^9}\right)[\text{Bcr-Abl}\cdot\text{G}]\right) - k_{\text{I2}}\left(\left(\frac{59}{10^9}\right)[\text{Bcr-Abl}^*]\right)G^m_{cell} + k_{-\text{I2}}\left(\left(\frac{59}{10^9}\right)[\text{Bcr-Abl}^*\cdot\text{G}]\right) \quad (21)$$

The last three equations, (19)-(21), describe the pharmacokinetics of Gleevec in the mouse (Figure 4). G^m_{IP}, G^m_{bl}, and G^m_{cell} represent the mass of Gleevec in the intraperitoneal cavity (IP), blood (bl), and cell, respectively. U represents the injection rate of the drug into the animal, and is approximated by an impulse function. The numerical factor $(10^9/59)$ converts between mass units and nanomolar

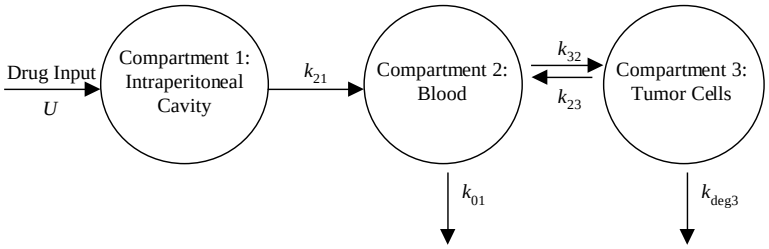

FIGURE 4. Pharmacokinetic model for Gleevec in the mouse. Gleevec is injected into the intraperitoneal (IP) cavity. We assume a mouse body weight of 25 grams to arrive at an initial Gleevec dosage of 0.00125 g [29]. The blood then delivers the drug to the tumor cells located on the left flank of the mouse.

concentration units; the molecular weight of Gleevec is 590, and the apparent volume of distribution was calculated to be 0.1 L using data from [29] and [21] and standard principles of pharmacokinetics [41].

Equations (19)-(21) are necessary to compare simulation results with experimental in vivo data from mouse models of CML available in the literature [29]. In these experiments, Gleevec is administered either orally (liquid form) or intraperitoneally, after which it is absorbed into the blood. The blood then delivers drug to the tumor cells, located on the left flank of the mouse. Both oral and intraperitoneal administration lead to rapid absorption into the blood.

Simulation results of individual species by themselves cannot be used to compare the model to experiment; concentration-time data for individual species are not available. On the other hand, relative data, i.e. the ratio of phosphorylated Bcr-Abl molecules after Gleevec administration to phosphorylated Bcr-Abl molecules before Gleevec administration, is available [29]. In addition, pharmacokinetic data for Gleevec in the mouse is available in [21]. As a result, the following output model was used to compare our mechanistic model, equations (11)-(21), to experimental data:

$$y_1 = \frac{[\text{Bcr-Abl*}]_{t>0}}{[\text{Bcr-Abl*}]_{t=0}} \tag{22}$$

$$y_2 = \frac{G_{bl}^m}{59\frac{g}{mol}L} \tag{23}$$

Equation (22) represents the percentage of phosphorylated Bcr-Abl molecules after administration of Gleevec at time $t = 0$, while equation (23) represents the concentration of Gleevec in the blood in units of mol/L. The value of [Bcr-Abl*] at time $t = 0$ is not known precisely. However, experimental gel data in [21] suggests that in the absence of Gleevec, most Bcr-Abl molecules exist in the phosphorylated state. Consequently, initial values for both [Bcr-Abl] and [Bcr-Abl*] were chosen such that the ratio [Bcr-Abl*]/[Bcr-Abl] was as close to one as possible.

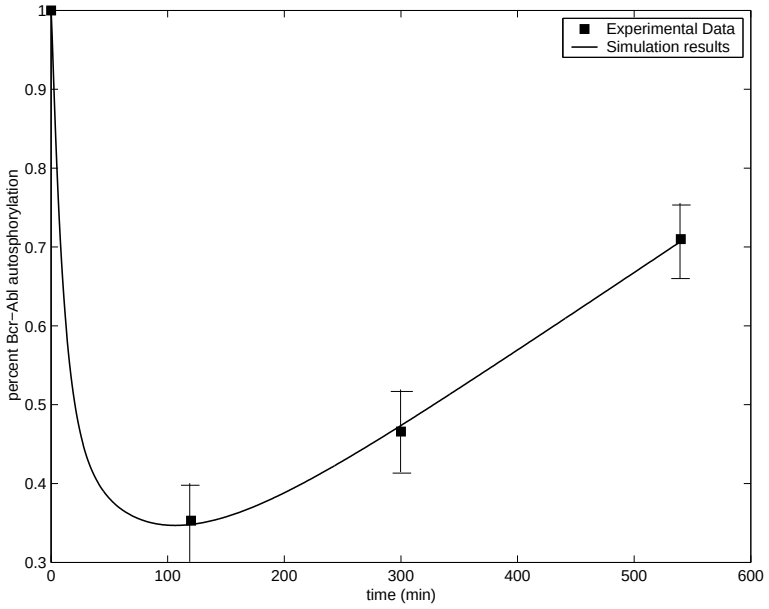

FIGURE 5. Best fit of equations (11)-(21) to data. Error bars were determined separately from the experiment. Gel experiments were obtained from the authors of [29], and the percent error computed as the standard deviation of the band intensities divided by the average intensity.

3. **Parameter Estimation.** Numerical values for the parameters in Table 1 were established from: 1) published values for the particular reaction, 2) published values for similar reactions in different systems, and 3) concentration-time curves for our model fitted to experimental data from [29] and [21] using least squares optimization.

To fit simulated concentration-time curves to experimental data, a hybrid parameter search algorithm was employed, based on differential evolution (DE) for global searching [45], in combination with a local search algorithm provided in MATLAB. DE is a population based direct search algorithm having the same general schema as a conventional genetic algorithm (GA), but is more efficient for optimization of a real-valued multimodal function. To further guarantee the optimality of the estimated parameters, after the termination of the DE algorithm, a local search is started from the approximate solution that the DE reaches. The local search algorithm used here is a trust region based conjugate gradient method implemented in the Matlab Optimization Toolbox; details can be found in [4]. The best fit criterion was taken to be minimization of unweighted least squares error, based on variability data provided by the author of ref. [21] (personal communication). Matlab was used to implement the overall scheme for parameter estimation and simulation.

Due to the large size of the parameter space, only certain combinations of parameters likely to be identifiable were allowed to vary; the rest were held fixed. Adjustable parameters were chosen based on the following criteria. We first fixed parameters with values known directly from the literature (Table 1). We then identified those parameters found in combination with other parameters as sums

	Parameter	Value	Units	Parameter Type	Source
1	k_1	0.048	$\text{nM}^{-1}\ \text{min}^{-1}$	2	[9,44]
2	k_{-1}	0.06	min^{-1}	3	
3	$k_{1\text{A}}$	3.5	$\text{nM}^{-1}\ \text{min}^{-1}$	3	
4	$k_{-1\text{A}}$	0.036	min^{-1}	3	
5	$k_{1\text{B}}$	0.006	$\text{nM}^{-1}\ \text{min}^{-1}$	2	[9,44]
6	$k_{-1\text{B}}$	$0.00849 \pm 1.09\times10^{-5}$	min^{-1}	4	
7	k_2	0.0032	$\text{nM}^{-1}\ \text{min}^{-1}$	2	[32]
8	k_{-2}	0.186	min^{-1}	2	[32]
9	k_{auto}	0.48	min^{-1}	2	[47]
10	k_{ph}	0.42	min^{-1}	2	[33]
11	k_{deph1}	0.000268	min^{-1}	3	
12	k_{deph2}	0.022	min^{-1}	3	
13	k_{I1}	0.006	$\text{nM}^{-1}\ \text{min}^{-1}$	1	[40]
14	$k_{\text{-I1}}$	$40\times k_{\text{I1}}$	min^{-1}	1	[40]
15	k_{I2}	0.0002	$\text{nM}^{-1}\ \text{min}^{-1}$	1	[40]
16	$k_{\text{-I2}}$	$7000\times k_{\text{I2}}$	min^{-1}	1	[40]
17	S_0	$0.0148 \pm 1.15\times10^{-5}$	nM/min	4	
18	S_1	0.0024	nM/min	3	
19	S_2	1.8×10^{-5}	nM/min	3	
20	k_{deg1}	0.0018	min^{-1}	1	[16]
21	k_{deg2}	0.042	min^{-1}	3	
22	k_{deg3}	$1.00 \pm 6.30\times10^{-2}$	min^{-1}	4	
23	[ATP]	7	nM	3	
24	k_{21}	3	min^{-1}	3	[21]
25	k_{32}	$0.00935 \pm 1.23\times10^{-5}$	min^{-1}	4	[21]
26	k_{23}	$0.00221 \pm 3.86\times10^{-5}$	min^{-1}	4	[21]
27	k_{01}	0.0042	min^{-1}	1	[49]

TABLE 1. Parameter values for Bcr-Abl signaling model. Parameter types are as follows. 1: values obtained from the literature, based on experimental data related to the particular reaction, with sources given. 2: estimated using known experimental data from a similar, but unrelated, reaction. 3: unidentifiable model parameters. 4: identifiable model parameters fitted to produce best least squares error of simulation results to known experimental data. These are given along with their computed standard deviations.

or products, as in equations (12)-(16), e.g. the term $k_{1A}k_{\text{auto}}/(k_{-1A}+k_{\text{auto}})$ in equation (12). Since the individual parameters in these combinations do not appear in other parts of the model, we redefined each combination as a lumped parameter to simplify analysis:

$$\alpha_1 = \frac{k_{1\text{A}}k_{\text{auto}}}{k_{-1\text{A}}+k_{\text{auto}}},\ \alpha_2 = \frac{k_{\text{ph}}k_2}{k_{\text{ph}}+k_{-2}}, \tag{24}$$

Next, a numerical sensitivity analysis was performed to test identifiability of the remaining adjustable parameters. Individual parameters and the lumped parameters

in (24) were adjusted sequentially up to one order of magnitude above and below an initial estimated value to discern if the change would have an effect on simulation output. Those that produced no change in output were fixed. The actual values of these numerically unidentifiable parameters are not of biological importance to this study, so fixing them is justified given that the resulting least squares fit is acceptable. In the end, a reduced set of adjustable, numerically identifiable parameters was obtained. These were then allowed to vary during the hybrid DE - local search parameter fitting runs.

After fitting, parameter standard deviations (Table 1) were computed using data variability noted earlier as follows. Given N measurements and p unknown parameters to be identified, the covariance matrix of the estimated parameters was calculated from [2]:

$$\hat{V} = \hat{\sigma}^2 J^T J$$

where $\hat{\sigma}^2$ is the estimate of the variance of measurement computed as $\frac{1}{N-p}$ times the sum squares of residual error between the measurement and the simulated output using the estimated parameters, and J is the $N \times p$ sensitivity matrix that contains the derivatives of the model outputs with regard to the estimated parameters at every instant of the observation. J was obtained by a forward approximation of the derivatives.

4. **Simulation Results.** Equations (11)-(21) with equations (22) and (23) as the output were simulated and fit to experimental data [21,29]. A good fit was obtained only when the parameter k_{deg3} became large (Table 1). This parameter represents nonspecific clearance of Gleevec from a cell, for example degradation of the drug within the cell itself or drug efflux from the cell mediated by membrane transporter proteins such as P-glycoprotein (Pgp) and Multidrug Resistance Protein (MRP) [1,42,50]. The large value of this parameter has an important biological implication: it predicts that, during blast crisis, mechanisms responsible for drug degradation and/or clearance from a cell dramatically reduce the effectiveness of Gleevec.

5. **Phase Plane Analysis.** The crucial first step in all Bcr-Abl mediated signaling events is the initial binding of ATP to Bcr-Abl. Mathematically, this is reflected in the fact that equations (11) and (12) drive all other equations in the system. Inspection of (11) and (12) reveals that the only coupling that occurs between these two equations and other equations in the system arises from only two terms appearing in (11), the $k_{-\text{I2}}$[Bcr-Abl·G] term and the k_{deph1}[Bcr-Abl*] term. Assuming that these two terms are negligible decouples (11) and (12) from the rest of the equations. This allows for a phase plane analysis of (11) and (12), leading to relevant biological conclusions in this limiting situation.

The phase plane portrait of equations (11) and (12) is presented in Figure 6; the corresponding null clines are given by

$$[\text{Bcr-Abl}] = \frac{k_{-1}}{k_1[\text{ATP}] + k_{\text{deg1}} + k_{\text{I1}}[G]}[\text{Bcr-Abl·ATP}] + \frac{S_0}{k_1[\text{ATP}] + k_{\text{deg1}} + k_{\text{I1}}[G]} \tag{25}$$

$$[\text{Bcr-Abl}] = \frac{k_{1\text{A}} k_{\text{auto}}}{k_1[\text{ATP}](k_{-1\text{A}} + k_{\text{auto}})}[\text{Bcr-Abl·ATP}]^2 + \frac{k_{-1}}{k_1[\text{ATP}]}[\text{Bcr-Abl·ATP}] \tag{26}$$

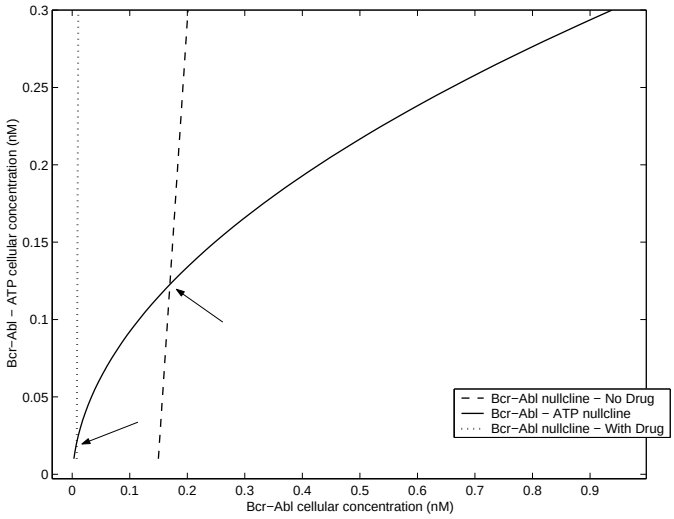

FIGURE 6. Phase plane analysis of equations (11) and (12) neglecting the $k_{\_I2}$[Bcr-Abl·G] and the k_{deph1}[Bcr-Abl*] terms in equation (11). The solid line indicates the [Bcr-Abl] null cline in which no drug has been added to the system. The dotted line indicates the [Bcr-Abl] null cline with a Gleevec concentration of 1 mM. The effect of the drug is to move the fixed point to a lower value of [Bcr-Abl] and [Bcr-Abl·ATP], as expected. Arrows point to the location of fixed points.

The figure shows that, before drug therapy begins, the concentration of [Bcr-Abl] and [Bcr-Abl·ATP] reach levels of approximately 0.2 nM and 0.12 nM, respectively. Analytically, this fixed point is given by

$$[\text{Bcr-Abl·ATP}] = \frac{-b + \sqrt{b^2 - 4ac}}{2a} \tag{27}$$

where $a = \dfrac{{}^{k}1\text{A}\,{}^{k}\text{auto}}{k_1[\text{ATP}]({}^{k}\_1\text{A} + {}^{k}\text{auto})}$, and

$$b = \frac{k_{-1}}{k_1[\text{ATP}]} - \frac{k_{-1}}{k_1[\text{ATP}] + k_{\text{deg1}} + k_{\text{I1}}[\text{G}]}$$

$$c = -\frac{S_0}{k_1[\text{ATP}] + k_{\text{deg1}} + k_{\text{I1}}[\text{G}]}$$

and is stable by linear stability analysis. Adding Gleevec to the system causes this fixed point to move to lower values of [Bcr-Abl] and [Bcr-Abl·ATP], as expected.

Because the location of the fixed point is affected by the concentration of Gleevec, we plot the fixed point as a function of Gleevec concentration (Figures 7A and 7B). These figures show that a 1 μM cellular concentration of Gleevec is enough to drop the concentration of Bcr-Abl by over 90%, whereas a slightly higher concentration of Gleevec is required to achieve the same 90% reduction in the concentration of Bcr-Abl·ATP. Greater amounts of Gleevec have a minimal effect. It should be noted, however, that Gleevec cannot reduce the concentration of either species to zero. This is consistent with the mechanism of action of Gleevec; the drug acts as

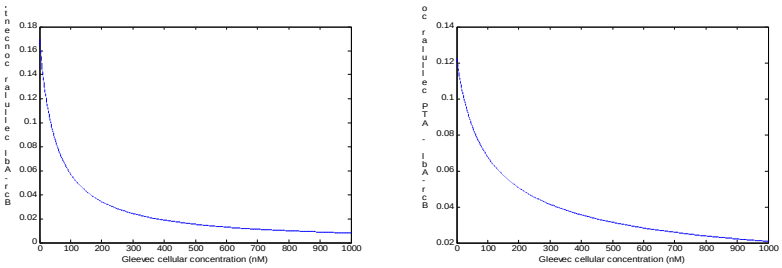

FIGURE 7. (a)-(b). Bcr-Abl and Bcr-Abl·ATP fixed points as a function of Gleevec (STI571) concentration. A low mM cellular concentration of Gleevec appears sufficient to effectively reduce the amount of Bcr-Abl and Bcr-Abl·ATP in a cell. This conclusion, however, should be regarded as the minimal amount required for drug efficacy because of assumptions made in the analysis (see text).

a competitive inhibitor of ATP (Figure 3). It does not directly affect the synthesis of Bcr-Abl.

6. **Discussion.** Simulation results suggest that, during blast crisis, the nonspecific clearance of Gleevec from a cell is very rapid, reducing effectiveness of the drug. If this model prediction is correct, it suggests an approach to enhance the effectiveness of Gleevec: delineate the mechanism(s) responsible for clearance of the drug, and then develop other therapies to block this process to give in combination with Gleevec.

One possible mechanism for drug clearance is efflux from the cell mediated by membrane transporter proteins such as Pgp or MRP. Experimental reports have already demonstrated that in cell lines resistant to Gleevec, this mechanism plays an important role [30]. Simulation results presented here predict a new effect. Because cells used in the experiment to which our model was fitted [29] were acutely treated with Gleevec, i.e. they had not been exposed to Gleevec prior to the experiment, the model predicts that cellular drug clearance mechanisms have a significant effect from the beginning of Gleevec therapy, not just after therapy has begun.

It must be noted, however, that although the cells used in the experiment to which our model was fitted had not been exposed to Gleevec, they were obtained from patients in blast crisis who had been previously treated with another drug, busulfan. As a result, two scenarios exist that might explain the appearance of cellular drug clearance mechanisms. First, drug clearance might be insignificant in the beginning, but disease progression to blast crisis and/or exposure to drug therapies, regardless of which drug is used, might cause an increase in clearance. Alternatively, clearance mechanisms might be present in leukemia cells from the onset of disease. Experimental evidence supports the latter scenario [7] for the specific case of clearance by drug efflux proteins; cells from newly diagnosed CML patients were shown to already display drug efflux activity at levels much higher than in non-leukemic cells. In sum, model results predict that cellular drug clearance mechanisms is significant during blast crisis, and it is speculated that this phenomenon might be present from the very beginning of the disease.

The model presented here has been fitted to mouse Bcr-Abl autophosphorylation data. Similar data are not available for the human because Bcr-Abl obtained from human clinical material rapidly degrades during experimental procedures required to isolate the protein [23]. Relevant results for the human can still be reached, however, despite the fact that we fit our model to mouse data. First, both human and murine Bcr-Abl must initially undergo autophosphorylation in order to become activated. The mechanism of autophosphorylation is likely the same, although this must be regarded as an assumption. Second, the catalytic domains of murine and human Bcr-Abl are identical except for a single amino acid substitution at position 336 in the Abl subunit. Gleevec binds to this catalytic domain, but binding is unaffected by the amino acid substitution [40]. As a result, the dynamics of Gleevec in mouse models and in humans with regard to Bcr-Abl inhibition is also likely the same. Thus, results presented here, that cellular drug clearance mechanisms are significant during blast crisis, are expected to carry over into the human.

Finally, results from a phase plane analysis show that a minimal cellular concentration of Gleevec is required for drug efficacy. This conclusion, however, was made under two assumptions, that the terms $k_{\_I2}$[Bcr-Abl·G] and k_{deph1}[Bcr-Abl*] were negligible. The first assumption, that $k_{\_I2}$[Bcr-Abl·G] is negligible, is equivalent to Gleevec behaving as a "perfect" drug, one with infinite affinity for its target. In other words, Gleevec binds Bcr-Abl, but never releases. In reality Gleevec is not "perfect." Neglecting the second term, k_{deph1}[Bcr-Abl*], ignores an input source to the equation for Bcr-Abl, equation (11). Therefore, the overall effect of ignoring these two terms is that the cellular concentration of Bcr-Abl is underestimated. As a result, the conclusion reached above, that a 1 mM Gleevec cellular concentration is needed to effectively lower the level of Bcr-Abl, should be regarded as the minimal amount required for drug efficacy.

REFERENCES

[1] Aszalos, A. and D. D. Ross, Biochemical and clinical aspects of efflux pump related resistance to anti-cancer drugs. *Anticancer Res.* **18** (1998), 2937-2944.

[2] Bard, Y. *Nonlinear Parameter Estimation,* Academic Press, New York, 1974.

[3] Barnes, D. J. and J. V. Melo, Cytogenetic and molecular genetic aspects of chronic myeloid leukaemia, *Acta Haematol.* **108** (2002), 180-202.

[4] Branch, M. A., T. F. Coleman, and Y. Li, A subspace, interior, and conjugate gradient method for large-scale bound-constrained minimization problems, *SIAM J. Sci. Comput.* **21** (1999), 1-23.

[5] Brasher, B. B. and R. A. Van Etten, c-Abl has high intrinsic tyrosine kinase activity that is stimulated by mutation of the Src homology 3 domain and by autophosphorylation at two distinct regulatory tyrosines, *J. Biol. Chem.* **45** (2000), 35631-35637.

[6] Buchdunger, E., C. L. Cioffi, N. Law, D. Stover, S. Ohno-Jones, B. J. Druker, and N. B. Lydon, Abl protein-tyrosine kinase inhibitor STI571 inhibits in vitro signal transduction mediated by c-Kit and platelet-derived growth factor receptors, *J. Pharmacol. Exp. Ther.* **295** (2000), 139-145.

[7] Carter, A., E. J. Dann, T. Katz, Y. Shechter, A. Oliven, R. Regev, E. Eytan, J. M. Rowe1 and G. D. Eytan, Cells from chronic myelogenous leukaemia patients at presentation exhibit multidrug resistance not mediated by either MDR1 or MRP1, *Br. J. Haematol.* **114** (2001), 581-590.

[8] Chai, S. K., G. L. Nichols, and P. Rothman, Constitutive activation of JAKs and STATs in Bcr-Abl expressing cell lines and peripheral blood cells derived from leukemic patients, *J. Immunol.* **159** (1997), 4720-4728.

[9] Chen, G., M. D. Porter, J. R. Bristol, M. J. Fitzgibbon, and S. Pazhanisamy, Kinetic mechanism of the p38-alpha MAP kinase: phosphoryl transfer to synthetic peptides, *Biochemistry* **39** (2000), 2079-2087.

[10] Chopra, R., Q. Q. Pu, and A. G. Elefanty, Biology of Bcr-Abl, *Blood Rev.* **13** (1999), 211-229.

[11] Cohen, M. H., G. Williams, J. R. Johnson, J. Duan, J. Gobburu, A. Rahman, K. Benson, J. Leighton, S. K. Kim, R. Wood, M. Rothmann, G. Chen, K. M. U, A.M. Staten, and R. Pazdur, Approval Summary for imatinib mesylate capsules in the treatment of chronic myelogenous leukemia, *Clin. Cancer Res.* **5** (2002), 935-942.

[12] Cuervo, A. M. and J. F. Dice, Lysosomes, a meeting point of proteins, chaperones, and proteases, *J. Mol. Med.* **76** (1998), 6-12.

[13] Daley, G. Q., R. A. Van Etten, and D. Baltimore, Induction of chronic myelogenous leukemia in mice by the P210 bcr/abl gene of the Philadelphia chromosome, *Science* **247** (1990), 824-830.

[14] Danial, N. N., A. Pernis, and P. B. Rothman, Jak-STAT signaling induced by the v-abl oncogene, *Science* **269** (1995), 1875-1877.

[15] Deininger, M. W. N., J. M. Goldman, and J. V. Melo, The molecular biology of chronic myeloid leukemia, *Blood* **96** (2000), 3343-3356.

[16] Dhut, S., T. Chaplin, and B. D. Young, BCR-ABL and BCR proteins: biochemical characterization and localization, *Leukemia* **4** (1990), 745-50.

[17] Druker, B. J., S. Tamura, E. Buchdunger, S. Ohno, G. M. Segal, S. Fanning, J. Zimmermann, and N. B. Lydon, Effects of a selective inhibitor of the Abl tyrosine kinase on the growth of Bcr-Abl positive cells, *Nat. Med.* **2** (1996), 561-566.

[18] Druker, B. J., STI571 (Gleevec) as a new paradigm for cancer therapy, *Trends. Mol. Med.* **8** (2002), S14-S18.

[19] Eaves, C. J., J. Cashman, and A. C. Eaves, Defective regulation of leukemic hematopoiesis in chronic myeloid leukemia, *Leuk. Res.* **22** (1998), 1085-1096.

[20] Fader, S., M. Talpaz, Z. Estrov, S. O'Brien, R. Kurzrock, and H. M. Kantarjian, The biology of chronic myeloid leukemia, *N. Engl. J. Med.* **341** (1999), 164-172.

[21] Gambacorti-Passerini, C., R. Barni, P. le Coutre, M. Zucchetti, G. Cabrita, L. Cleris, F. Rossi, E. Gianazza, J. Brueggen, R. Cozens, P. Pioltelli, E. Pogliani, G. Corneo, F. Formelli, and M. D'Incalci, Role of alpha1 acid glycoprotein in the in vivo resistance of human Bcr-Abl-positive leukemic cells to the Abl inhibitor STI571, *J. Natl. Cancer Inst.* **92** (2000), 1641-1650.

[22] Glickman, M. H. and A. Ciechanover, The ubiquitin-proteasome proteolytic pathway: destruction for the sake of construction, *Physiol. Rev.* **82** (2002), 373-428.

[23] Gorre, M. E., M. Mohammed, K. Ellwood, N. Hsu, R. Paquette, P. N. Rao, and C. L. Sawyers, Clinical resistance to STI-571 cancer therapy caused by BCR-ABL gene mutation or amplification, *Science* **293** (2001), 876-80.

[24] Heinrich, M. C., D. J. Griffith, B. J. Druker, C. L. Wait, K. A. Ott, and A. J. Zigler, Inhibition of c-kit receptor tyrosine kinase activity by STI571, a selective tyrosine kinase inhibitor, *Blood* **96** (2000), 925-932.

[25] Holyoake, T. L., X. Jiang, M. W. Drummond, A. C. Eaves, and C. J. Eaves, Elucidating critical mechanisms of deregulated stem cell turnover in the chronic phase of chronic myeloid leukemia, *Leukemia* **16** (2002), 549-558.

[26] Ilaria Jr., R. L. and R. A. Van Etten, P210 and P190(Bcr/ABL) induce the tyrosine phosphorylation and DNA binding activity of multiple specific STAT family members, *J. Biol. Chem.* **271** (1996), 31704-31710.

[27] Jørgensen, H. G. and T.L. Holyoake, A comparison of normal and leukemic stem cell biology in chronic myeloid leukemia, *Hematol. Oncol.* **19** (2001), 89-106.

[28] Kantarjian, H. M., S. O'Brien, J. E. Cortes, S. A. Giralt, M. B. Rios, J. Shan, F. J. Giles, D. A. Thomas, S. Faderl, M. De Lima, G. Garcia-Manero, R. Champlin, R. Arlinghaus, and M. Talpaz, Imatinib mesylate therapy for relapse after allogeneic stem cell transplantation for chronic myelogenous leukemia, *Blood* **100** (2002), 1590-1595.

[29] le Coutre, P. L., L. Mologni, L. Cleris, E. Marchesi, E. Buchdunger, R. Giardini, F. Formelli, and C. Gambarcorti-Passerini, In vivo eradication of human BCR/ABL-positive leukemia cells with an ABL kinase inhibitor, *J. Natl. Cancer. Inst.* **91** (1999), 163-168.

[30] Mahon, F., F. Belloc, V. Lagarde, C., F. Moreau-Gaudry, J. Reiffers, J. M. Goldman, and J. V. Melo, MDR1 gene overexpression confers resistance to imatinib mesylate in leukemia cell line models, *Blood* **101** (2003), 2368-2373.

[31] Mandanas, R. A., D. S. Leibowitz, K. Gharehbaghi, T. Tauchi, G. S. Burgess, K. Miyazawa, H. N. Jayaram, and H. S. Boswell, Role of p21 ras in p210 bcr-abl transformation of murine myeloid cells, *Blood* **82** (1993), 1838-1847.

[32] Matsuda, M., S. Ota, R. Tanimura, H. Nakamura, K. Matuoka, T. Takenwawa, K. Nagashima, and T. Kurata, Interaction between amino-terminal SH3 domain of Crk and its natural target proteins, *J. Biol. Chem.* **271** (1996), 14468-14472.

[33] Mayover, T. L., C. J. Halkides, and R. C. Stewart, Kinetic characterization of CheY phosphorylation reactions: comparison of P-CheA and small molecule phosphodonors, *Biochemistry* **38** (1999), 2259-2271.

[34] Nichols, G. L., M. A. Raines, J. C. Vera, L. Lacomis, P. Tempst, and D. W. Golde, Identification of Crkl as the constitutively phosphorylated 39-kD tyrosine phosphoprotein in chronic myelogenous leukemia cells, *Blood* **84** (1994), 2912-2918.

[35] Oda, H., C. Heaney, J. R. Hagopian, K. Okusa, J. D. Griffin, and B. J. Druker, Crkl is the major tyrosine phosphorylated protein in neutrophils from patients with chronic myelogenous leukemia, *J. Biol. Chem.* **269** (1994), 22925-22928.

[36] Puil, L., J. Liu, G. Gish, G. Mbamalu, D. Bowtell, P. G. Pelicci, R. Arlinghaus, and T. Pawson, Bcr-Abl oncoproteins bind directly to activators of the Ras signaling pathway, *EMBO J.* **13** (1994), 764-773.

[37] Raitano, A. B., J. R. Halpern, T. M. Hambuch, and C. L. Sawyers, The Bcr-ABL leukemia oncogene activates Jun kinase and requires Jun for transformation, *Proc. Natl. Acad. Sci. USA* **92** (1995), 11746-11750.

[38] Rowley, J. D., A new consistent chromosomal abnormality in chronic myelogenous leukaemia identified by quinacrine fluorescence and Giemsa staining, *Nature* **243** (1973), 290-293.

[39] Sawyers, C. L., Chronic myeloid leukemia, *N. Engl. J. Med.* **340** (1999), 1330-1340.

[40] Schindler, T., W. Bornmann, P. Pellicena, W. T. Miller, B. Clarkson, and J. Kuriyan, Structural mechanism for STI-571 inhibition of abelson tyrosine kinase, *Science* **289** (2000), 1938-1942.

[41] Shargel, L. and A. B. C. Yu, *Applied Biopharmaceutics and Pharmacokinetics,* McGraw-Hill/Appleton & Lange, 1999

[42] Sharom, F. J., The P-glycoprotein efflux pump: how does it transport drugs? *J. Membr. Biol.* **160** (1997), 161-175.

[43] Shet, A. S., B. N. Jahagirdar, and C. N. Verfaillie, Chronic myelogenous leukemia: mechanisms underlying disease progression, *Leukemia* **16** (2002), 1402-1411.

[44] Skamnaki, V. T., D. J. Owen, M. E. M. Noble, E. D. Lowe, G. Lowe, N. G. Oikonomakos, and L. N. Johnson, Catalytic mechanism of phosphorylase kinase probed by mutational studies, *Biochemistry* **38** (1999), 14718-14730.

[45] Skorski, T., P. Kanakaraj, M. Nieborowska-Skorska, M. Z. Ratajczak, S.-C. Wen, G. Zon, A. M. Gewirtz, B. Perussia, and B. Calabretta, Phosphatidylinositol-3 kinase activity is regulated by BCR/ABL and is required for the growth of Philadelphia chromosome-positive cells, *Blood* **86** (1995), 726-736.

[46] Storn, R. and K. Price, Differential Evolution A simple and efficient heuristic for global optimization over continuous spaces, *J. Global Optim.* **11** (1997), 341-359.

[47] Tawa, P. and R. C. Stewart, Kinetics of CheA autophosphorylation and dephosphorylation reactions, *Biochemistry* **33** (1994), 7917-7924.

[48] ten Hoeve, J., R. B. Arlinghaus, J. Q. Guo, N. Heisterkamp, and J. Groffen, Tyrosine phosphorylation of Crkl in Philadelphia+ leukemia, *Blood* **84** (1994), 1731-1736.

[49] Tomasson, M. H., I. R. Williams, R. Hasserjian, C. Udomsakdi, S. M. McGrath, J. Schwaller, B. Druker, and D. G. Gilliland, TEL/PDGFbR induces hematologic malignancies in mice that respond to a specific tyrosine kinase inhibitor, *Blood* **93** (1999), 1707-1714.

[50] Twentyman, P. R., Transport proteins in drug resistance: biology and approaches to circumvention, *J. Intern. Med. Suppl.* **740** (1997), 133-137.

[51] Warmuth, M., S. Danhauser-Riedl, and M. Hallek, Molecular pathogenesis of chronic myeloid leukemia: implications for new therapeutic strategies, *Ann. Hematol.* **78** (1999), 49-64.

[52] Zhou, J. and J. A. Adams, Participation of ADP dissociation in the rate-determining step in cAMP-dependent protein kinase, *Biochemistry* **36** (1997), 15733-15738.

Received November 2002; revised June 2003.

E-mail address: pep@chem.ucla.edu, joed@cs.ucla.edu